Rapid heating and cooling in two-dimensional Yukawa systems

Yan Feng,* Bin Liu, and J. Goree
Department of Physics and Astronomy, The University of Iowa, Iowa City, Iowa 52242, USA
(Received 14 May 2008; published 26 August 2008)

Simulations are reported to investigate solid superheating and liquid supercooling of two-dimensional systems with a Yukawa interparticle potential. Motivated by experiments where a dusty plasma is heated and then cooled suddenly, we track particle motion using a simulation with Langevin dynamics. Hysteresis is observed when the temperature is varied rapidly in a heating and cooling cycle. As in the experiment, transient solid superheating, but not liquid supercooling, is observed. Solid superheating, which is characterized by solid structure above the melting point, is found to be promoted by a higher rate of temperature increase.

DOI: 10.1103/PhysRevE.78.026415 PACS number(s): 52.27.Lw, 52.27.Gr, 68.35.Rh, 64.70.D−

I. INTRODUCTION

A superheated solid is a solid at temperatures above its melting point [1], and a supercooled liquid is a liquid at temperatures below its melting point [2]. Compared with the supercooled liquid (which is commonly found in many substances including glasses, colloidal suspensions [3,4], and water [5]), superheated solids are very rare. Indeed, solid superheating was once thought to be impossible [6], because the thermal energy will break down the bonds between atoms if the temperature is higher than the melting point.

In the literature, we find reports of two general methods for solid superheating. First, if metal or ice is heated with an ultrafast heating method [7,8], then solid superheating can occur for a short time. (A limited lifetime of the superheated solid, before melting, is an indication of what has been called transient solid superheating [9].) Second, solid superheating experiments have been reported for some specially fabricated samples. For example, if lead is precipitated into aluminum [10] or lead layers are sandwiched between aluminum layers [11], then the lead can stay in a solid state at temperatures higher than the melting point of lead for a long time. (A long lifetime of the superheated solid is an indication of what has been called metastable solid superheating [9].)

In a recent experiment [12], we observed transient solid superheating in a two-dimensional (2D) suspension in a dusty plasma using rapid laser heating, as reviewed in Sec. IV. In dusty plasmas, small particles of solid matter are electrically charged and suspended in plasmas. Due to their mutual Coulomb repulsion, when confined electrically these particles can self-organize in a so-called plasma crystal, in which the particles are arranged in space like molecules in a crystal or liquid [13–18]. Since dusty plasmas, like colloidal suspensions [3,4], allow direct imaging of particles using video microscopy, they allow particle tracking and measurement of microscopic structure [13–16]. This allows direct comparison of experiment and molecular dynamics simulations [16], since both the experiment and simulations yield the same measurable quantities: time series for particle positions and velocities. Performing a simulation requires specifying the interparticle potential. One advantage of dusty plasma experiments with a 2D suspension is that the form of the interparticle potential is known. It has been demonstrated experimentally that the binary interparticle interaction is modeled by a Yukawa potential [19] when particles are confined to a single layer that is perpendicular to ion flow, as in our experiment.

Hysteresis occurs in many physical and other systems. Physical examples include magnetic [20] and electric polarization [21] hysteresis, when time-varying fields are applied to a condensed matter sample. Hysteresis also occurs in other fields like biology [22] and economics [23]. A hysteresis diagram is typically prepared by combining time series measurements for two quantities, for example measurements of magnetization M and applied field H combined into a single graph with M as the vertical and H as the horizontal axis. For solid superheating experiments, temperature is the customary horizontal axis [10]. For the vertical axis, in our recent experiment [12], we used the defect fraction, while previous experimenters used some externally measured parameter derived typically from an x-ray diffraction image [10].

Here we report results from a molecular dynamics simulation, for conditions similar to those in our experiment [12]. Molecular dynamics simulations are idealized models of an experiment because they use simple physics without some of the peculiarities of the experiment. We use a 2D Langevin simulation method to model the entire time series for an experiment, including both heating and subsequent cooling. (Details are described in Sec. II.) A previous paper [16] reported results for a simulation of cooling.

Our simulation results, Sec. V, reveal a hysteresis similar to the one observed in the experiment [12]. As in the experiment, we search for the signatures of solid superheating and liquid supercooling, and we observe the former but not the latter. The general agreement between the experiment [12] and the simulation results presented here is helpful in demonstrating that the experiment observations are merely due to simple physics processes, and not to peculiarities of the experiment such as non-Maxwellian velocity distribution or anisotropy [12]. The simulation allows varying some parameters such as friction and initial defect fraction that are not easily adjustable over a wide range in the experiment, and this helps in gaining insight into the experiment. These results may also be helpful in understanding other 2D experimental systems, including electrons on the surface of liquid helium [24], granular fluids [25], and colloidal suspensions [4].

*yan-feng@uiowa.edu

II. SIMULATION

We performed Langevin dynamical simulations. We used a binary interparticle interaction with a Yukawa pair potential,

$$\phi(r_{i,j}) = Q^2(4\pi\epsilon_0 r_{i,j})^{-1} \exp(-r_{i,j}/\lambda_D), \quad (1)$$

where Q is the particle charge, λ_D is the screening length, and $r_{i,j}$ is the distance between particles i and j. Equilibrium Yukawa systems can be classified by the values of Γ and κ [26,27]. Here,

$$\Gamma = Q^2/(4\pi\epsilon_0 a k_B T) \quad (2)$$

and $\kappa \equiv a/\lambda_D$, where T is the particle kinetic temperature, $a \equiv (n\pi)^{-1}$ is the Wigner-Seitz radius [28], and n is the areal number density. The length scale a is related to the lattice constant b (for a defect-free crystal) by $a = b/1.9046$. Our simulation includes 16 384 particles in a rectangular box of dimensions $137.5b \times 119.1b$. Time scales of interest are characterized by the inverse of the nominal plasma frequency, $\omega_{pd}^{-1} = (Q^2/2\pi\epsilon_0 m a^3)^{-1/2}$ [28], where m is the particle mass. (In the experiment [12], $a = 0.45$ mm and $\omega_{pd}^{-1} = 30$ ms.)

We integrate the Langevin equation of motion for each particle. This equation is

$$m\ddot{\mathbf{r}}_i = -\nabla \sum \phi_{ij} - \nu m \dot{\mathbf{r}}_i + \zeta_i(t), \quad (3)$$

with frictional drag $\nu m \dot{\mathbf{r}}_i$ and a random force $\zeta_i(t)$. Particles are allowed to move in a single 2D plane. Note that we retain the inertial term on the left-hand side in Eq. (3), unlike some Brownian-dynamics simulations of overdamped colloidal suspensions [29], where it is set to zero.

The random force $\zeta_i(t)$ is assumed to have a Gaussian distribution with zero mean. The magnitude of the random force, characterized by the width of its Gaussian distribution, is chosen to attempt to achieve a desired target temperature T_{ref} according to the fluctuation-dissipation theorem [30,31],

$$\langle \zeta_i(0)\zeta_i(t)\rangle = 2m\nu k_B T_{ref}\delta(t), \quad (4)$$

where the delta function $\delta(t)$ indicates that the random force $\zeta_i(t)$ is local in time.

The fluctuation-dissipation theorem [30] is useful for many physical systems, including, for example, Brownian motion. It relates dissipation to microscopic fluctuations and the temperature in thermal equilibrium. This dissipation, which occurs at a microscopic scale, is of interest also for nonequilibrium behavior. However, the fluctuation-dissipation theorem does not accurately model all nonequilibrium systems, for example some experiments where energy is pumped in [32]. Therefore, we do not expect exact agreement between our nonequilibrium experiment and a simulation that assumes the fluctuation-dissipation theorem.

Our simulation mimics our monolayer dusty plasma experiment [12] in the use of a 2D monolayer with a Yukawa potential with similar values of parameters Γ and κ, but it differs from the experiment in at least three ways. First, the heating and friction are explicitly coupled by Eq. (4), which is slightly different from the experiment (which is a driven-dissipative system [12,33], as described in Sec. IV). Second, it uses periodic boundary conditions to model an infinite system. Third, it uses a larger particle number.

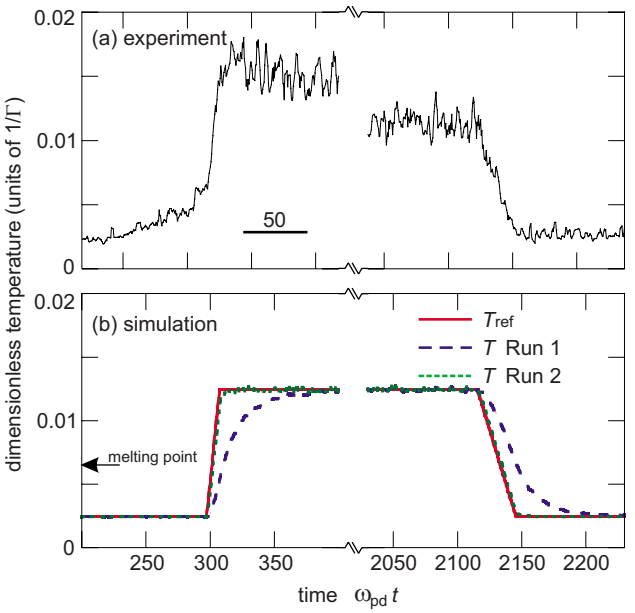

FIG. 1. (Color online) Time series for temperature. (a) For the experiment, the observed temperature was calculated from the mean-square velocity fluctuation. (b) For the simulation, the target temperature time series (red solid line) was prescribed. The resulting observed temperature, computed from mean-square velocity fluctuations, are shown for run 1 with low friction (blue dashed line) and run 2 with high friction (green dotted line).

The input parameters specified for the simulation include κ, ν/ω_{pd}, and the target Γ_{ref} [calculated from a target temperature T_{ref}, charge Q, and the Wigner-Seitz radius a using Eq. (2)]. Here we will prescribe a wave form for $T_{ref}(t)$ rather than hold it constant, in order to mimic the rapid heating and cooling in the experiment. When we change T_{ref}, ν remains constant. This will cause the random force $\zeta_i(t)$ to become stronger (if T_{ref} is increased) or weaker (if T_{ref} is decreased) according to Eq. (4).

We initialized the simulation by starting particles at positions that would lead to the desired defect fraction, and then running the simulation for an initialization time $372\omega_{pd}^{-1}$. At time $t=0$, defined as the end of this initialization, we began recording time series of data for particle positions and velocities.

The time series we specified for the target temperature T_{ref} is presented in Fig. 1. The target temperature was at first held steady at a baseline (below the melting point) until about $t = 300\omega_{pd}^{-1}$. Then we began ramping $T_{ref}(t)$ upward at a constant rate, with a rise time of $10\omega_{pd}^{-1}$ to a maximum value of T_{ref}, which we specified well above the melting point. This procedure was intended to mimic the rapid heating in the experiment. Next, we held $T_{ref}(t)$ constant for a duration of $1806\omega_{pd}^{-1}$, nearly matching the duration of steady laser heating in the experiment. Then, we ramped $T_{ref}(t)$ back down to its baseline in a fall time of $30\omega_{pd}^{-1}$, to mimic the rapid cooling of the experiment. Finally, we held $T_{ref}(t)$ constant, recording data until $t = 3325\omega_{pd}^{-1}$. This final stage corresponds to

the long period of recrystallization observed in the experiment [12].

Here we review other details of our simulation. We used the Langevin integrator of Gunsteren and Berendsen [31]. A time step of $0.037\omega_{pd}^{-1}$ and periodic boundary conditions were used. We truncated the Yukawa potential at radii beyond $12a$, with a switching function to give a smooth cutoff between $12a$ and $14a$ to avoid an unphysically sudden force when a particle moves a small distance.

We performed two simulations. Run 1 was intended to approximate the friction in the experiment, $\nu/\omega_{pd}=0.066$, corresponding to $\nu=2.2\ s^{-1}$ and $\omega_{pd}=33.3\ s^{-1}$. Run 2 had a tenfold higher friction, $\nu/\omega_{pd}=0.66$, corresponding to $\nu=22\ s^{-1}$. Both of these runs began with particles arranged in a solid structure having an initial defect fraction (concentration) of 0.027, similar to the experiment.

As a test, we repeated the simulations reported here with a different initial condition of a defect-free crystal. We found that the results are similar enough that our conclusions are unaffected by the initial defect fraction.

The time series for temperature in the experiment and simulations are presented in Fig. 1. In both cases, the observed temperature T is calculated from the measured values of the mean-square velocity fluctuations. The observed temperature time series from the simulation is similar to the temperature time series from our experiment for run 2, with the high friction. But at a lower friction in run 1, the temperature changes more slowly. As compared to run 2, the slow rate of temperature change in run 1 is due to a smaller random force $\zeta_i(t)$ from Eq. (4) when T_{ref} is changed.

The difference in the rate of change of temperature, for the simulation as compared to the experiment, is attributed to the different ways that heating and friction are related in the experiment (where they are independent) and simulation [where they are explicitly coupled through Eq. (4), as discussed above]. Because of this, it is difficult to match both the observed temperature time series $T(t)$ and gas friction ν in simulations. Our simple wave form for the target temperature $T_{ref}(t)$ allows us to match $T(t)$ or ν, but not both. Therefore, we will compare results for two cases: Run 1 where we match the friction ν, and run 2 where we nearly match the time series for observed temperature $T(t)$. Comparing these two runs will be useful in assessing the relative importance of friction and rate of temperature change for solid superheating.

III. DIAGNOSTICS

Here we introduce the diagnostics used to test for solid superheating and liquid supercooling. Our main result will be time series for two variables, which we will combine to construct a hysteresis diagram. One of these variables will be the observed temperature T. The other variable will be chosen from three structure indicators, which are calculated from the particle positions. First, we identify defects and calculate defect area fraction by calculating Voronoi diagrams [15]. Second, we measure the short-range translational order using the height of the first peak of the pair correlation function $g(r)$ [34]. Third, we measure the short-range orientational order

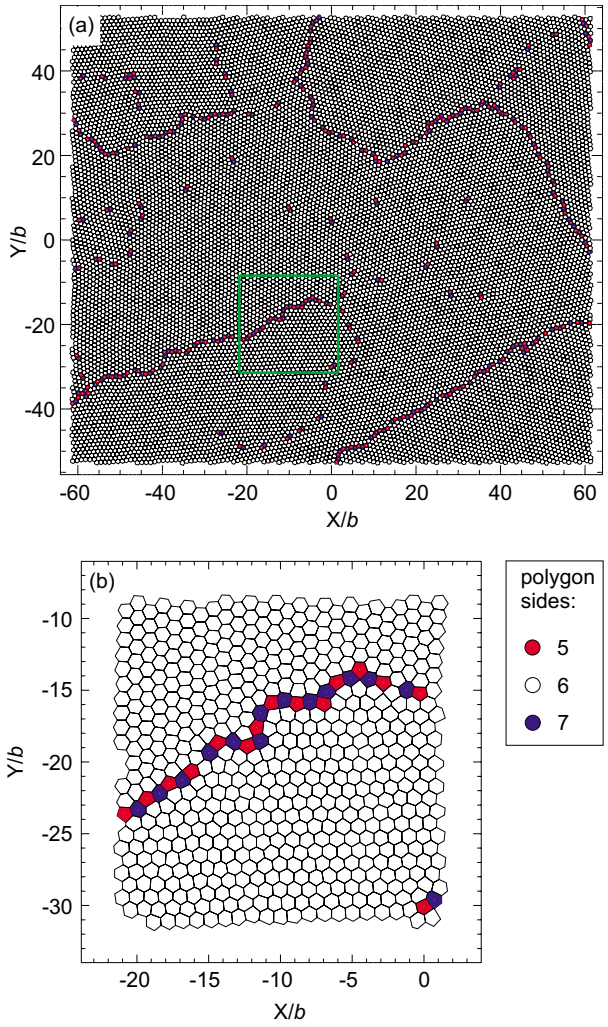

FIG. 2. (Color online) (a) Voronoi diagram calculated from our simulation data, before rapid heating when $\Gamma>400$. (b) Magnified view of the portion inside the green square in (a). For both panels, the horizontal and vertical dimensions are normalized by the lattice constant b. For both run 1, shown here, and run 2, the initial conditions had the same defect fraction 0.027. Note that, at this level of defect fraction, defects are arranged mainly in strings, forming domain walls that separate domains with different orientations. Due to the presence of these domains, G_θ is only 0.216.

using the bond-angular-order parameter G_θ [35]. We present a detailed explanation of these three structure indicators next.

A Voronoi diagram is calculated from particle positions of each frame [15]. Figure 2 shows the Voronoi diagram calculated for run 1 before rapid heating. In the case of a defect-free 2D crystal, the Voronoi diagram would include only six-sided polygons. When defects are present, they are identified by the presence of non-six-sided polygons, as in Fig. 2, where the number of sides is indicated by different colors. To reduce the information in a Voronoi diagram to a single parameter, we calculate the defect fraction as the ratio of the areas of all non-six-sided polygons to the area of the entire Voronoi diagram. The defect fraction can vary from zero for a defect-free crystal to roughly 0.3 for a liquid.

A feature that can be identified easily by examining Voronoi diagrams is the presence of different domains that

collectively form a polycrystalline solid. For run 1, in Fig. 2, we see that most defects are not distributed sparsely, but instead tend to self-organize by forming strings that serve as domain walls. In each domain, there is a crystalline region that has an angular orientation that is different from the next. Domains divided by domain walls are features also found in our experiment [12].

The pair correlation function $g(r)$ is calculated from particle positions; and it can be reduced to a single parameter by measuring the height of its first peak. This height serves as a measure of the local translational order, and it can vary upward from roughly 2 for a liquid to arbitrarily large values for a solid, depending on temperature and defects. This parameter generally does not exhibit significant jumps as disorder increases, so that we do not use it to distinguish liquid from solid.

The bond-angular-order parameter G_θ [35] is calculated from angles between nearby particles. The value of G_θ varies from zero for a gas to unity for a defect-free crystal. For a solid, G_θ is less than unity if there are defects. The calculation of this parameter, like the defect fraction and the height of the first peak of $g(r)$ listed above, involves an average over a sample area, which in the case of our simulation is the entire simulation box. In previous simulations with slowly varying temperature [35], it was found that G_θ served as a useful indicator of melting because of a distinctive jump in its value. This jump occurs at G_θ=0.45 for different 2D physical systems, including a 2D Yukawa system, which is useful for quantifying the melting point. However, we find that G_θ is very sensitive to the presence of domains within the sample area, because terms entering the calculation of G_θ for one domain can cancel those from another domain, so that the value of G_θ depends on the size of the sample area and how many domains it includes. The larger the number of domains enclosed, the smaller the value of G_θ. Therefore, G_θ will be more useful when melting a defect-free crystal with only a single domain than for melting a polycrystalline solid like the one in Fig. 2 and in the experiment [12].

Of the three structure indicators listed above, we choose the defect fraction as the variable to present in the vertical axis of the hysteresis diagram. This choice has the advantage that, unlike G_θ, it is not highly sensitive to the size of the sample area, and it has a slower response to a change in temperature than the height of the first peak of $g(r)$ [12]. Our hysteresis diagram will therefore have defect fraction and temperature as the vertical and horizontal axes, respectively.

The type of hysteresis that is observed here is rate dependent. Consequently, the general appearance of a hysteresis diagram will depend on how rapidly the temperature is varied. We illustrate this in the sketch in Fig. 3. If temperature is varied rapidly, the hysteresis will be most extreme, while if it is varied infinitely slowly in a quasistatic process, hysteresis will vanish and the curve will retrace itself exactly when melting and solidifying.

The signature of solid superheating or liquid supercooling can be easily identified in a hysteresis diagram [12]. A horizontal row of data points across the melting point means that the temperature has changed across the melting point while the structure has not changed yet. This is sketched at the bottom and top of Fig. 3.

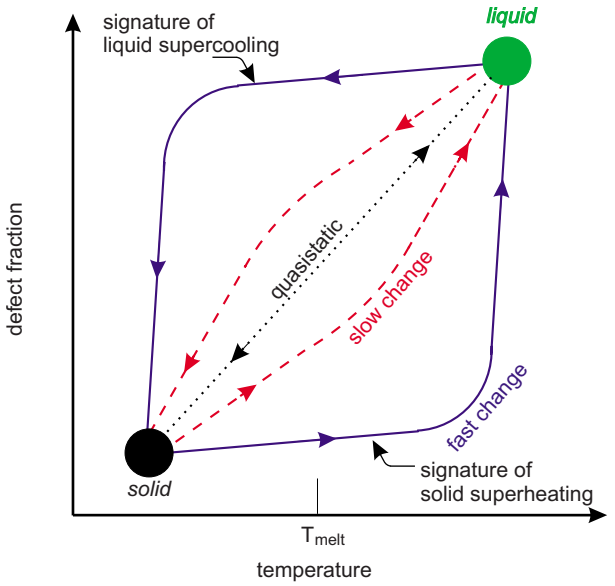

FIG. 3. (Color online) Sketch of a hysteresis diagram for a solid-liquid transition. The vertical axis, defect fraction, is a structure indicator. Hysteresis, if it occurs, may depend on the rate of temperature change. It is not expected if temperature is changed infinitely slowly in a quasistatic process.

To determine the melting point, we rely on the phase diagram, Fig. 6 in Ref. [36], for a 2D equilibrium Yukawa system. This phase diagram provides a curve in the Γ-κ parameter space. Using this curve is straightforward for our simulation because we specify κ, so that the curve directly yields the Γ (and therefore the temperature) for the melting point. We also use the same curve to determine the melting point for the experiment using the same procedure and an experimentally measured value for κ.

IV. REVIEW OF EXPERIMENT

Here we review the experiment reported in Ref. [12] and provide further discussion of its physics. A single horizontal layer of electrically charged polymer microspheres was electrically levitated in a glow-discharge plasma, forming what is called a dusty plasma. Viewing the suspension from above with a video camera, movies of particle motion were recorded. Initially, particles were self-organized in a nearly crystalline solid lattice. Particle motion was cooled by friction on the ambient rarefied neutral gas. Later, an external source of heating was applied suddenly. This heating source was a cw laser beam, rastered in a Lissajous pattern to give particles kicks at nearly random times [33,34]. In steady state, the particle kinetic temperature is determined by a balance of external laser heating and frictional gas drag cooling [12]. After applying the external heating for about 55 s, it was suddenly stopped. During the initial phase of external heating, the temperature increased rapidly, at about 20 000 K/s. After a delay of about 0.25 s the suspension melted, as judged by a change in defect fraction.

This delay was interpreted as an indication of solid superheating. An additional indication is the signature of solid

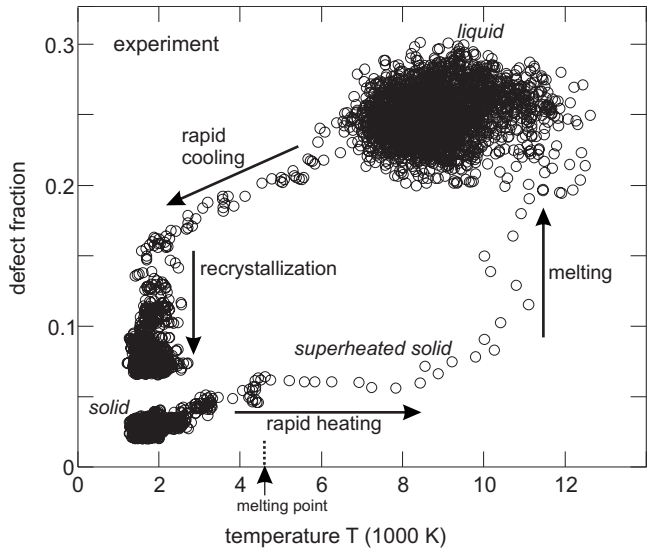

FIG. 4. Hysteresis diagram for the experiment. Time series for observed temperature T and defect fraction, both recorded at time intervals of 18 ms, were combined to produce this diagram. At the bottom, the horizontal row of data points crossing the melting point was interpreted in [12] as showing the signature of solid superheating. Reprinted from [12].

superheating that can be identified in the experimental hysteresis diagram, Fig. 4, as a horizontal row of about 15 data points. This row of data points begins at about the melting point, and continues to about 10 000 K, well above the melting point.

The solid superheating had a limited duration, which we interpret as an indication that it is a kind of transient solid superheating. In general, one could identify solid superheating as being either transient or metastable, depending on the duration of the solid structure after increasing the temperature above the melting point. The distinction between transient and metastable superheating has been previously mentioned in a review of the literature [9]. For our experiment, we judge the duration of the superheated solid by comparing its lifetime of about 0.25 s to another important time scale for particle motion: the period of oscillation corresponding to the Einstein frequency ω_E. Here ω_E has the usual meaning: it is the oscillation frequency that a charged particle's motion would have in a cage formed by all the other particles, if all the other particles were stationary. The Einstein frequency for our experiment can be estimated from a combination of our experimental measurement of the plasma frequency $\omega_{\mathrm{pd}}=33.3\ \mathrm{s}^{-1}$ and a previous simulation that provided a relationship between ω_{pd} and ω_E [28]. This yields an estimate in our experiment of $\omega_E=0.612\omega_{\mathrm{pd}}=20.4\ \mathrm{s}^{-1}$. The corresponding period of oscillation for the charged particle in the experiment is $\tau_E=2\pi/\omega_E=0.31$ s. Comparing now to the experimentally observed lifetime of about 0.25 s for the superheated solid, we find that the lifetime was only about one oscillation period, before melting occurred. Therefore, we interpret our experimental results as an indication of transient, not metastable, superheating.

The underlying reason for the solid superheating in the experiment is simple to understand, now that the time scales have been determined. Initially, in the solid below the melting point, particles are caged by their nearest neighbors. Caged particle motion in a solid consists mainly of oscillations, with a turning point located well within the cage. In a full period of oscillation, characterized by a τ_E, a particle's trajectory has two turning points. As rapid heating is suddenly applied, particles in the cage are accelerated, the cage distorts as other particles are also accelerated, and the enclosed particle can eventually decage and thereby generate a defect. In the experiment, the time indicated by the hysteresis diagram for this decaging to occur is about 0.25 s, about the same as $\tau_E=0.31$ s. Comparing these two values indicates that after sudden heating is applied, a particle typically decages after bouncing about twice in the cage. This short-lived stage of bouncing about twice before decaging corresponds to the transient superheated solid.

During the experiment, the single-layer particle suspension was not constrained in its size. In principle, its areal number density could vary in time. We calculated a time series for the areal number density, and we found that there was no significant expansion as the temperature increased. The areal number density remained constant within 1.5% during the experiment [12], despite very large temperature changes of an order of magnitude. It is interesting that despite the extreme softness of this suspension, its volume varies so little with temperature.

Another major result from our experiment was that the signature of liquid supercooling was lacking in the hysteresis diagram, Fig. 4. A horizontal row of data points extending below the melting point is absent in this hysteresis. Instead, the defect fraction drops dramatically as the temperature decreases. In Sec. V, for the simulation results, we will examine the hysteresis diagrams to determine whether the same signatures of solid superheating and liquid supercooling are present.

One feature of the hysteresis diagram that requires explanation is the gap in data points at the lower left of Fig. 4. This gap is due to the finite data-recording time in the experiment. After the initial rapid cooling, a very slow recrystallization takes place. During the recrystallization, crystalline domains gradually grow in size by merging with neighboring domains. The merging process is slow because a domain must rotate until its orientation aligned with a neighboring domain. This process becomes increasingly slow as the remaining domains become larger, as can be seen in the Voronoi movie from the experiment [12]. The camera in the experiment had a finite memory, allowing the recording of a movie limited to 100 s duration for the entire experiment. A similar gap will occur in the hysteresis diagram for the simulation data, Sec. V, because of the expense of running the simulation to the completion of the same slow recrystallization process.

Previous to our experiment [12], Knapek *et al.* reported another experiment [16] to study the recrystallization during cooling. They used a similar dusty plasma with a single-layer suspension of microspheres. They heated their suspension suddenly by applying an electrical pulse to wires. Using video microscopy, particle motion was recorded well after the pulse was completed, so that the experimenters observed the cooling process, but not the heating process. As in our

experiment [12], this cooling process included a rapid cooling followed by a slow recrystallization. Like us, they reported time series for temperature and defect fraction; they also reported correlation lengths as measures of orientational and translational order, serving roles similar to G_θ and height of the first peak of $g(r)$. They found that temperature decreases more rapidly than defect fraction [16], a result that we verified in [12]. They also found that orientational order drops much more slowly than translational order, and attributed this to the presence of domains in various orientations during the slow recrystallization process [16]. Our experiment differed by using laser heating, which did not disturb the particle layer severely. Because of this, we were able to record particle motion during both heating and cooling, allowing us to prepare hysteresis diagrams.

V. SIMULATION RESULTS

In our Langevin dynamical simulation, we found a hysteresis, as in the experiment [12]. The hysteresis diagrams were prepared by combining time series for observed temperature, Fig. 1(b) and defect fraction. The data in these time series were recorded at time intervals $0.37\omega_{\mathrm{pd}}^{-1}$. Numerical noise in the simulations was reduced below the level in the experiment by using a large number 16 384 particles in the simulation, about 15 times larger than in the experiment. As a result, the hysteresis curve is less noisy for the simulation than for the experiment. The two runs described below began with different initial particle positions, but the same defect fraction.

Recall that when we change T_{ref} in the simulation the friction ν remains constant, and the magnitude of the random force $\zeta_i(t)$ is changed according to Eq. (4). The observed temperature $T(t)$ will lag the target temperature $T_{\mathrm{ref}}(t)$, because of the time required for the random force to accelerate particles. This lag in the temperature change is seen in Fig. 1, especially for the low friction case, run 1.

A. Run 1: Low friction

For run 1 we found the hysteresis diagram of Fig. 5(a). For this run, the friction was as low as in the experiment, but the observed temperature changed at a slower rate.

The signature of solid superheating in the simulation for run 1 is not as clear as in the experiment. Examining the bottom of the hysteresis diagram, Fig. 5(a), we observe that the defect fraction begins to increase noticeably before the temperature has exceeded the melting point. The structure, as measured by defect fraction, is no longer the same as it was in the initial solid, although it more nearly resembles a solid than a liquid. A rapid increase in defect fraction ensues at temperatures somewhat higher than the melting point.

The weaker signature of solid superheating in the simulation might be due to the different temperature time series, as compared to the experiment. As shown in Fig. 1, the time series for observed temperature in experiment and run 1 do not match exactly. Since the hysteresis is rate dependent, a slower change in temperature will tend to lack a signature of solid superheating, as sketched in Fig. 3.

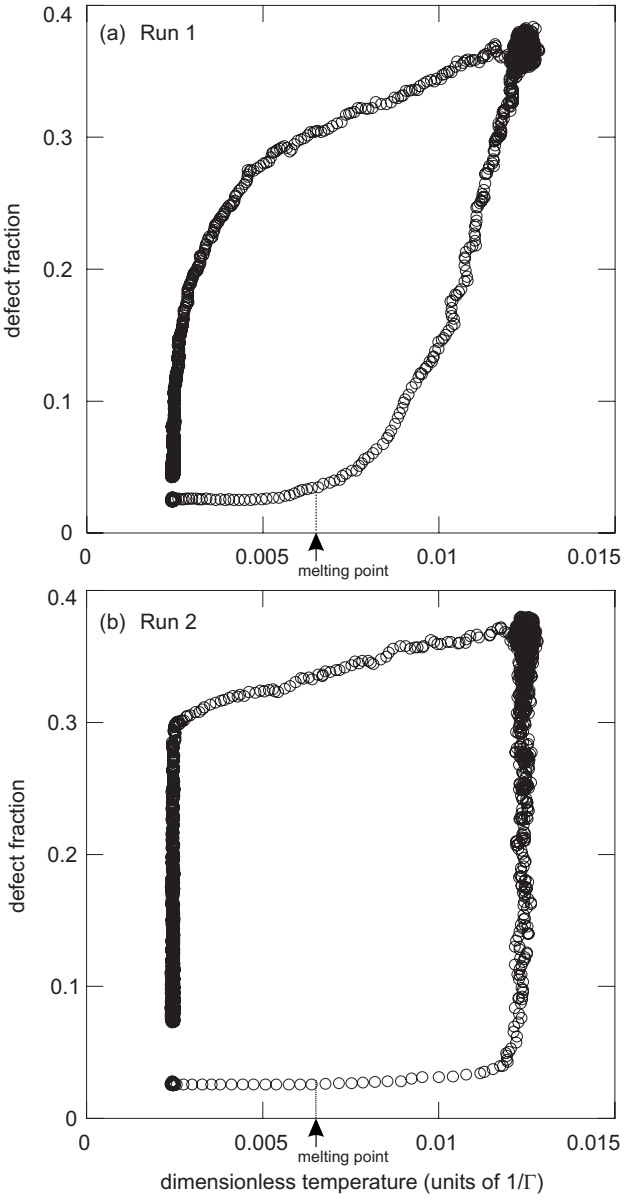

FIG. 5. Hysteresis diagrams for (a) run 1 and (b) run 2. In both runs, the same initial defect fraction and target temperature time series were used, but in run 1 a lower friction resulted in a slower rate of temperature change. These diagrams were made by combining time series for defect fraction and observed temperature T, recorded at a time interval of $0.37\omega_{\mathrm{pd}}^{-1}$.

The signature of liquid supercooling in run 1 is lacking, as it was in our experiment. Instead of remaining constant as the temperature decreases as would be required for supercooling, the defect fraction drops dramatically.

B. Run 2: Higher friction

For run 2 we found the hysteresis diagram of Fig. 5(b). For this run, the friction was ten times higher than in the experiment, but the observed temperature changed at about the same rate.

The signature of solid superheating for run 2 resembles the experiment more nearly than for run 1. This leads us to

conclude that a high rate of temperature change, as in run 2, is important for attaining solid superheating.

The signature of liquid supercooling remains lacking in run 2. This result for both simulation runs and the experiment suggests that liquid supercooling is not easily attained in this physical system, for the rate of temperature change that we explored here.

VI. DISCUSSION

We have simulated our rapid heating and cooling experiment [12]. We used a Langevin simulation of a 2D Yukawa system, with a temperature that was ramped in time by specifying a target temperature. By combining time series for observed values of temperature and defect fraction, we produced hysteresis diagrams. These diagrams allow an inspection for the signatures of solid superheating and liquid supercooling.

We draw three chief conclusions. First, the simulations are capable of producing hysteresis as in the experiment. The physics incorporated in the simulation is very simple, in comparison to the experiment which has more complications. Our finding that hysteresis arises in both the simulation and experiment indicates that the cause of the hysteresis is simple physics, and not a peculiarity of the experiment.

Second, in both the experiment and simulation, the signature of liquid supercooling was lacking. This result is of interest because it is an open question whether there can be any one-component 2D systems that behave like a supercooled liquid [4].

Third, we found that the hysteresis curve for simulation and experiment most nearly agree when the rate of temperature change is matched. Our simulation method, together with our choice of a time series for the target temperature $T_{\mathrm{ref}}(t)$, allowed us to match either the time series for observed temperature $T(t)$ or the friction ν for the experiment and simulation, but not both. We found that the hysteresis in the experiment was most nearly duplicated in the simulation run with the same rapid change of the observed temperature. This result leads us to conclude that a high rate of temperature change is an important requirement for attaining solid superheating.

ACKNOWLEDGMENTS

We thank F. Skiff for helpful discussions. This work was supported by NASA and DOE.

[1] X. M. Bai and M. Li, J. Chem. Phys. **123**, 151102 (2005).
[2] M. D. Ediger, C. A. Angell, and S. R. Nagel, J. Phys. Chem. **100**, 13200 (1996).
[3] E. R. Weeks *et al.*, Science **287**, 627 (2000).
[4] H. König *et al.*, Eur. Phys. J. E **18**, 287 (2005).
[5] R. S. Smith and B. D. Kay, Nature (London) **398**, 788 (1999).
[6] J. G. Dash, Rev. Mod. Phys. **71**, 1737 (1999).
[7] H. Iglev *et al.*, Nature (London) **439**, 183 (2006).
[8] J. W. Herman and H. E. Elsayed-Ali, Phys. Rev. Lett. **69**, 1228 (1992).
[9] R. W. Cahn, Nature (London) **323**, 668 (1986).
[10] L. Gråbæk, J. Bohr, H. H. Andersen, A. Johansen, E. Johnson, L. Sarholt-Kristensen, and I. K. Robinson, Phys. Rev. B **45**, 2628 (1992).
[11] L. Zhang, Z. H. Jin, L. H. Zhang, M. L. Sui, and K. Lu, Phys. Rev. Lett. **85**, 1484 (2000).
[12] Y. Feng, J. Goree, and B. Liu, Phys. Rev. Lett. **100**, 205007 (2008).
[13] H. M. Thomas and G. E. Morfill, Nature (London) **379**, 806 (1996).
[14] A. Melzer, A. Homann, and A. Piel, Phys. Rev. E **53**, 2757 (1996).
[15] R. A. Quinn and J. Goree, Phys. Rev. E **64**, 051404 (2001).
[16] C. A. Knapek, D. Samsonov, S. Zhdanov, U. Konopka, and G. E. Morfill, Phys. Rev. Lett. **98**, 015004 (2007).
[17] M. Rubin-Zuzic *et al.*, Nature (London) **2**, 181 (2006).
[18] C. L. Chan and L. I, Phys. Rev. Lett. **98**, 105002 (2007).
[19] U. Konopka, G. E. Morfill, and L. Ratke, Phys. Rev. Lett. **84**, 891 (2000).
[20] D. P. Norton *et al.*, Appl. Phys. Lett. **82**, 239 (2003).
[21] S. Priya and K. Uchino, J. Appl. Phys. **91**, 4515 (2002).
[22] J. J. Tyson and B. Novak, J. Theor. Biol. **210**, 249 (2001).
[23] R. Baldwin, Am. Econ. Rev. **78**, 773 (1988).
[24] C. C. Grimes and G. Adams, Phys. Rev. Lett. **42**, 795 (1979).
[25] P. M. Reis, R. A. Ingale, and M. D. Shattuck, Phys. Rev. Lett. **96**, 258001 (2006).
[26] H. Ohta and S. Hamaguchi, Phys. Plasmas **7**, 4506 (2000).
[27] K. Y. Sanbonmatsu and M. S. Murillo, Phys. Rev. Lett. **86**, 1215 (2001).
[28] G. J. Kalman, P. Hartmann, Z. Donkó, and M. Rosenberg, Phys. Rev. Lett. **92**, 065001 (2004).
[29] H. Löwen, J. Phys.: Condens. Matter **4**, 10105 (1992).
[30] R. K. Pathria, *Statistical Mechanics* (Pergamon Press, Oxford, 1972).
[31] W. F. van Gunsteren and H. J. C. Berendsen, Mol. Phys. **45**, 637 (1982).
[32] D. Lobaskin and S. Kehrein, J. Stat. Phys. **123**, 301 (2006).
[33] B. Liu and J. Goree, Phys. Rev. Lett. **100**, 055003 (2008).
[34] V. Nosenko, J. Goree, and A. Piel, Phys. Plasmas **13**, 032106 (2006).
[35] I. V. Schweigert, V. A. Schweigert, and F. M. Peeters, Phys. Rev. Lett. **82**, 5293 (1999).
[36] P. Hartmann, G. J. Kalman, Z. Donkó, and K. Kutasi, Phys. Rev. E **72**, 026409 (2005).